Enhanced Conductivity and Non-linear Voltage-Current Characteristics of Non-stoichiometric $BaTiO_3$ Ceramics

Journal:	*Journal of the American Ceramic Society*
Manuscript ID:	JACERS-28765.R1
Manuscript Type:	Article
Date Submitted by the Author:	14-Jan-2011

Complete List of Authors:	Beltran, Hector; University Jaume I, Inorganic and Organic Chemistry; Universidad Jaume I, Química Inorgánica y Orgánica Prades, Marta; Universidad Jaume I, Química Inorgánica y Orgánica Masó, Nahum Cordoncillo, Eloisa; Universty Jaume I, Inoeganic chemistry; Universidad Jaume I, Química Inorgánica y Orgánica West, Anthony; PREFERS PAPER COPY The University of Sheffield, Department of Engineering Materials; University of Sheffield, Dept of Engineering Materials

Keywords:	barium titanate, electrical properties, impedance spectroscopy

Enhanced Conductivity and Non-linear Voltage-Current Characteristics of Non-stoichiometric $BaTiO_3$ Ceramics

Héctor Beltrán*, Marta Prades*, Nahum Masó‡, Eloisa Cordoncillo* and Anthony R West‡

* Universitat Jaume I, Departamento de Química Inorgánica y Orgánica, Avda. Sos Baynat s/n, 12071 Castellón, SPAIN.

‡ Department of Materials Science and Engineering, University of Sheffield, Mappin Street, Sheffield, S1 3JD, UK.

Abstract

The electrical conductivity of both BaO-deficient and TiO_2-deficient $BaTiO_3$ ceramics shows non-ohmic, low field characteristics at temperatures > ~ 200 ^oC in contrast to stoichiometric $BaTiO_3$ for which the electrical conductivity is independent of applied voltage. The non-linearity is observed in both bulk and grain boundary resistances of ceramics that are both porous (~82%) and non-porous (~98%) and is not associated with interfacial phenomena such as Schottky barriers and memristors nor with charge injection from the electrodes. Results, shown as a function of time over the temperature range 200 to 750 °C with field gradients in the range ~ 0.5 to 20 Vmm^{-1}, indicate that an excited state is reached that is time-, temperature- and field-dependent. This effect appears to be caused by departures from local electroneutrality in the defect structure of non-stoichiometric $BaTiO_3$ which are reduced by electron transfer on application of a *dc* bias, leading to a more conducting, low-level excited state in which holes associated with underbonded oxygens, presumably as O^- ions, are the principal charge carriers. Ceramics gradually return to their ground state in two stages on removal of the *dc* bias and the conductivity decreases overall by 2-3 orders of magnitude.

Introduction

The electrical properties of resistive materials in bulk form generally show linear voltage-current, V-I, behaviour at small applied voltages although at high voltages, insulating materials exhibit dielectric breakdown.[1] For materials in which conduction takes place by a hopping mechanism, of either ions or electrons, the conductivity can be modelled using random walk theory[2] and the effect of a small *dc* voltage is simply to apply a slight bias to the random motion of the conducting species, leading to a net drift in a particular direction. A small *dc* bias is insufficient to force ions or electrons to move; consequently, the V/I response obeys Ohm's Law.

In contrast to bulk properties which obey Ohm's Law, non-linear characteristics are commonly associated with interfacial effects, such as electrode-sample contacts which give rise to Schottky barriers.[1] There is also current interest in memristor effects in which, for the specific case of TiO_2 / $TiO_{2-\delta}$ interfaces, coupled electronic and ionic charge transfer occurs across the interface giving rise to non-linear phenomena.[3]

We have recently reported three examples of hopping electronic conduction in bulk ceramics of acceptor-doped $BaTiO_3$ (BT) that exhibit non-linear characteristics at low field and at temperatures in the range ~140 to ~650 ºC.[4-6] The dopants were Zn^{2+}, Mg^{2+} and Ca^{2+} which substituted for Ti^{4+} in the octahedral sites of the perovskite structure, with concentrations in the range 0.003 to 3 mole%. Both bulk and grain boundary conductivities increased by 1 to 2 orders of magnitude, at a rate that was dependent on temperature, on applying a *dc* bias in the range ~ 0.5 to 20 Vmm^{-1} at the same time as the *ac* impedance measurements were made. On removal of the *dc* bias, conductivities gradually returned to their original values. In all three cases, the dopants may be regarded as divalent acceptors that substitute for tetravalent Ti and are compensated by oxygen vacancy creation. Similar effects were not seen when Ca^{2+} replaced Ba^{2+} as an isovalent dopant.[6]

In the defect structure of divalent acceptor-doped BT, charge compensation is achieved by the creation of an equal number of oxygen vacancies adjacent to the acceptor ions, giving highly polar defect complexes, written ideally as eg $Mg_{Ti}'' - V_O^{\bullet\bullet}$, in which, using Kroger-Vink notation, $'$ and $^{\bullet}$ refer to charges of –1 and +1, respectively. It was proposed that charge polarisation in the defect complexes could be reduced by internal electron transfer, leading to low level, and more highly conducting, excited states. The key to this process appears to be underbonded oxide ions in the immediate vicinity of the defect complexes.

Although the electron affinity for the reaction $O + e^- \rightarrow O^-$ is negative, the electron affinity to add a second electron, $O^- + e^- \rightarrow O^{2-}$, is positive (in the gas phase) and the O^{2-} ion is stabilised in the solid state only by the high lattice energies of crystal structures. For underbonded O^{2-} ions in the vicinity of polar defect complexes, the stabilisation of the O^{2-} ions may be much reduced giving the possibility of easy ionisation to form O^- ions. The energy required to ionise these O^{2-} ions may be provided readily by application of a *dc* voltage, especially if the *dc* voltage across the entire sample takes the form initially of a high potential gradient at the electrode-sample interface.

Evidence for this mechanism was obtained from impedance measurements and in particular, from data analysis using the M'' formalism, which indicated that a nucleation and growth process was involved in forming the excited state.[4,5] The volume fraction of the excited state regions was found to increase with time until eventually, the entire sample was in the excited state.

There have been no other reports of non-linear bulk resistance phenomena at low fields in either pure or doped BT and clearly, it is essential to determine the conditions under which such an effect occurs. Also, as far as we are aware, no other material has been reported to show this effect. Here we show that, whereas linear bulk V–I behaviour is shown by stoichiometric, undoped $BaTiO_3$, non-stoichiometric BT containing a deficiency of either Ti or Ba, also shows non-linear enhanced conductivity on application of a small *dc* bias. The results can be interpreted by extending the polar defect cluster model proposed earlier for acceptor-doped BT.

Strategy for Materials Synthesis and Ceramic Fabrication

A major difficulty in evaluating composition-property relations in BT-based electroceramics concerns compositional control of high density ceramics. There is a vast literature on BT-based ceramics but it is commonly the case that compositions are not accurately stoichiometric. Thus, a slight excess of TiO_2 above the 1:1 BaO to TiO_2 ratio is often present together with sintering aids such as SiO_2. In addition, it is often suspected that contamination from the milling media occurs. Samples may be slightly oxygen non-stoichiometric, especially if quenched from high temperatures, whereas if they are cooled more slowly, then gradients in oxygen concentration may result giving rise to core-shell structures. Dopants/impurities may also be present/added either deliberately or inadvertently.

1

If the goal of a particular programme of work requires preparation of high density ceramics with optimised properties, then accurate control of composition, free from a number of additives, may have to be sacrificed. If, on the other hand, accurate compositional control is required so as to facilitate proper investigation of composition-property relations, it may be necessary to forego the fabrication of high density ceramics provided the presence of a certain level of porosity does not have a major influence on properties.

Our strategy falls into the second category. We work with high purity chemicals and avoid the use of mechanical milling. It is then certainly possible to obtain ceramics with > 80% density but which rarely achieve full density. Nevertheless, they are perfectly acceptable for most electrical property measurements, particularly conductivity. In addition, for the present study, samples were prepared from two entirely different sets of chemicals and used two very different synthesis routes. The fact that the resulting properties were largely independent of synthesis route and chemicals used but did vary greatly with composition indicated that composition was the main variable in controlling the properties of samples.

We have not attempted chemical analysis of samples since the properties were largely independent of chemicals used and synthesis route. In addition, the levels of non-stoichiometry in BaO-deficient and TiO_2-deficient samples were very small and would be difficult to determine accurately by chemical analysis methods; in particular, it would be extremely difficult to determine accurately the oxygen content of the non-stoichiometric samples. Our approach, therefore, has been to use high purity chemicals and work to avoid contamination as much as possible. We do not use sintering aids although it is much more difficult to prepare high density ceramics. However, we feel that this strategy is justified by the results which show high sensitivity of the electrical properties to composition.

Experimental

Samples of three compositions, BT, $BaTi_{0.99}O_{2.98}$ and $Ba_{0.99}TiO_{2.99}$, were prepared by two routes, by sol-gel synthesis using chemicals and procedures described previously[7] and by solid state reaction. For the sol-gel method, powders were decomposed and given a final firing at 1400 °C for 2 hours after which they were ground, pressed into pellets, fired at increasing temperatures with a final firing at 1400 ºC for 12 h in air and then cooled naturally by switching off the furnace. During firing, pellets were placed on a bed of sacrificial powder of the same composition in Pt foil boats. The purpose of the sacrificial powder was to prevent possible contamination on reaction of the pellets with Pt.

For solid state synthesis, powders of $BaCO_3$ (99.98% pure, Aldrich; dried at 180 °C overnight prior to weighing) and TiO_2 (99.9% pure, Sigma-Aldrich; dried at 800 °C overnight prior to weighing) were mixed, pressed into pellets and placed on sacrificial powder of the same composition in Pt foil boats. Initial firing was at 1000 °C for 6h to eliminate CO_2 after which the pellets were ground, repressed, fired at 1250 °C for 6 hours, ground, pressed isostatically at 200 MPa, given a final firing at 1400 °C for 12h in air and then cooled slowly by switching off the furnace. We avoided the use of ball milling systems and media to mix samples since these are prone to the introduction of contaminants; all samples were, instead, hand-mixed and milled using an agate mortar and pestle. Using our normal procedures (10-15 min mixing, with acetone added periodically to form a paste), typical pellet densities after firing sol-gel derived samples were ~82%, Table I. Given the necessity to demonstrate that the results presented here were not, in some way, influenced by ceramic porosity, samples prepared by the solid state route used more extended hand-milling times (~1h) and in this way, pellets with densities as high as 98% were achieved, Table I. The electrical conductivity results, especially field-dependent conductivities, were found to be similar for samples of a given composition for pellets densities in the range ~82 to 98%, indicating that the electrical properties were essentially uninfluenced by ceramic porosity.

The phases present were analyzed by X-Ray Powder Diffraction, XRD, using a Stoe StadiP Diffractometer, Cu$K\alpha_1$ radiation with a linear position-sensitive detector. Lattice parameters were determined from X-ray powder data by least-squares refinement for reflections in the range $15 < 2\theta < 70^\circ$, using the software WinXPow version 1.06. Angle correction was carried out using an external silicon standard.

Scanning electron micrographs (SEMs) of the pellet surfaces were taken on a SEM JEOL 7001F model, equipped with a spectrometer for energy dispersive analysis of X-rays (EDX), using the following operation parameters: probe current 0.05 pA, acceleration voltage 15 kV, measuring time

20 s and working distance 10 mm. The samples for microstructure determination and microanalysis were deposited on an Al holder and coated with graphite.

For electrical property measurements, pellets were coated with electrodes made from Pt paste that was decomposed and hardened by heating to 900 ºC. Impedance measurements used an Agilent 4294A impedance analyser over the frequency range 40 Hz to 7 MHz and from room temperature to 900 ºC. The *ac* measuring voltage was 100 mV; in addition, a *dc* bias in the range 0.5-15 V was applied for selected experiments. Impedance data were corrected for the overall pellet geometry and for the blank capacitance of the conductivity jig. Resistance and capacitance data are, therefore, reported in units of Ωcm and Fcm^{-1}, respectively. While these data for the bulk component, R_1 and C_1, essentially represent the bulk resistivity and permittivity (corrections for ceramic porosity were not made), the grain boundary data are not corrected for the grain boundary geometry. It would therefore be a serious error to refer to the grain boundary data, corrected only for overall pellet geometry, as resistivities and permittivities. We therefore present all resistance and capacitance data in units of Ωcm and Fcm^{-1} to show that they are corrected for pellet geometry but do not refer to the grain boundary data as resistivities and permittivities. The ratio between the sample permittivity and the permittivity of free space ($\varepsilon'/\varepsilon_0$) is the dielectric constant (*k*) or relative permittivity (ε_r'). We prefer use of the term relative permittivity since the alternative term, dielectric constant, tends to be restricted to frequency-independent bulk permittivities, sometimes also known as the limiting high frequency permittivity, ε_∞', or capacitance, C_∞, which is an intrinsic property of the sample.

Results

The non-stoichiometric BT ceramics that were studied contained either a deficiency of TiO_2, with nominal formula $BaTi_{0.99}O_{2.98}$ or a deficiency of BaO, $Ba_{0.99}TiO_{2.99}$. Samples were phase-pure by

XRD with the tetragonal BT structure. Ceramic densities were 82-98%, depending on processing and firing conditions (discussed later), Table I. Grain sizes, determined by SEM were 20-150 μm, Fig 1, Table I. Sol-gel samples showed comparable grain size, ~20-150 μm, independently of the composition whereas in solid-state samples the grain size decreased from $Ba_{0.99}TiO_{2.99}$ to BT and $BaTi_{0.99}O_{2.98}$. There was no evidence of variation in Ba/Ti ratios nor of the occurrence of any secondary phases by EDX. It was concluded, therefore, that both non-stoichiometric samples were single phase solid solutions. Since the perovskite structure of BT contains no suitable space for interstitial cations, it is assumed that the solid solution mechanism(s) responsible for the variable composition of the non-stoichiometric samples is a vacancy mechanism, with vacancies on both the oxygen and Ba/Ti sublattices. To prove this experimentally would be extremely difficult given the 3 low vacancy concentrations but, given that solid solutions do form, there appears to be no alternative mechanism.

Direct evidence for solid solution formation was provided by fixed-frequency plots of relative permittivity against temperature, Fig 2. These showed that the Curie temperature, T_C, associated with the tetragonal to cubic phase transition decreased from 135 ºC (sol-gel) and 133 °C (solid state) for stoichiometric BT to 129 and 128 ºC with deficiencies of TiO_2 and BaO, respectively, Table I. The similarity in results from two entirely different sets of samples and prepared from different starting materials is evidence that the permittivity maximum, ε'_{max}, passes through a maximum for stoichiometric BT and decreases with deficiency of other Ba or Ti. The ε'_r data above T_C showed linear Curie–Weiss plots (Fig 2c,d) with T_0 values independent of measuring frequency; the value of T_C–T_0 was greater for Ba-rich samples than for stoichiometric and Ti-rich samples, Table I.

We note that a range of values for T_C of BT is quoted in the literature, but there is no accepted consensus as to the 'ideal' value, nor until now, convincing explanation for the variations in T_C. It is also the case that the BT that formed the basis of the literature reports was often not accurately stoichiometric but frequently had a small variation in the Ba:Ti ratio, together with the presence of sintering aids. Data obtained on our samples, Fig 2, indicate that T_C may vary by at least 7 ^{o}C, depending on the Ba:Ti ratio and this may contribute to the origin of the discrepancies in the literature data. It is generally accepted in the literature that a certain level of non-stoichiometry can occur, especially for BaO-deficient compositions in which the temperature of the cubic-hexagonal phase transition at ~1470 °C appears to be sample- and, therefore, composition-dependent. Present results, indicating a level of nonstoichiometry of at least 1% to either side of the BT composition, are therefore consistent with variations in literature T_C data; further studies to determine accurate solid solution limits and their possible temperature-dependence are desirable but are beyond the scope of this work.

Impedance measurements were used to characterise the electrical microstructure of ceramics using the standard techniques and data analysis methodology of impedance spectroscopy. A selection of typical impedance data for stoichiometric BT prepared by both sol-gel (pellet density 82%) and solid state (pellet density 90%) methods, with measurements taken both before and after application of a *dc* bias of 10V is shown in Fig 3. First, consider the data without an applied *dc* bias.

There are two components in the impedance complex plane plot of the sol-gel sample (a), a high-frequency arc (inset) with approximate resistance R_1~6 kΩcm, which is attributed to the sample grains and a much larger, lower frequency arc with R_2~360 kΩcm, attributed to the grain boundaries. In the solid state sample, there are again two components (d), but they are less-well resolved, and have comparable resistances of ~100–200 kΩcm. Assignment of the two impedance arcs to grain and grain boundary regions is supported by presentation of the same impedance data as spectroscopic Z"/M" plots, Fig 3 (b,e); the largest peak in the M" plot corresponds to the region of the sample with the smallest capacitance and therefore, to the sample grains.[8] This M" peak coincides with the high frequency peak or shoulder in the Z'' plots and therefore, R_1 represents the bulk resistance of the sample. For both samples, the impedance data may be represented ideally by an equivalent circuit containing two parallel RC elements in series, Fig 3d(inset).

Capacitance data can be calculated from the maxima in the Z''/M'' plots, using the relation: $2\pi fRC = 1$, but are seen more directly in plots of capacitance C' against frequency, as shown for the same data in Figs 3(c,f). All samples and measurements show a high frequency plateau at ~30 $pFcm^{-1}$ which represents the bulk capacitance, C_1, (or C_∞), of the samples. Such values are typical of BT ceramics above the Curie temperature with relatively high permittivity, ε_r' of ~340. A dispersion occurs at frequencies below ~10^5 to 10^6 Hz with clear evidence of a second, but less well resolved, low frequency plateau, C_2, at ~1 $nFcm^{-1}$ in (c) and ~0.4-0.5 $nFcm^{-1}$ in (f). The values of C_2 are 20–30 times the value of C_1 and therefore, C_2 is attributed to thin grain boundary regions of the samples.

The effect of a *dc* bias of 10V on the impedance response of stoichiometric BT is also shown in Fig 3. Very little dependence is seen: R_1, R_2, C_1 and C_2 are essentially unchanged for the sol-gel sample; for the solid state sample, R_1 and R_2 show a small decrease, but C_1 is unchanged and C_2 shows a small increase.

From the impedance data, Fig 3(a,b,d,e), values of the bulk, σ_1 and grain boundary, σ_2 conductivities were extracted and are shown in Arrhenius format in Fig 4. There is a significant difference in the bulk conductivities of the sol-gel and solid state samples but for both samples the application of a *dc* bias had almost no effect on the magnitudes of either bulk or grain boundary conductivities. The reason for the difference in bulk conductivities of sol-gel and solid state samples is not known.

For non-stoichiometric $BaTiO_3$, the impedance data are very different with and without *dc* bias, Figs 5-10; both R_1 and R_2 are much reduced and are time-dependent with a *dc* bias, Figs 5,8. The temperature-dependence of the capacitance C', was readily obtained by replotting impedance data as log C′ vs log f, Figs 5(c,f),8(c,f); although the real, resistive part of the impedance was too high to measure with the available instrumentation for temperatures below ~300 ºC, capacitance data were readily obtained and show temperature dependence characteristic of paraelectric behaviour above T_c, Fig 2. For the grain boundary, it was unclear from the impedance data whether C_2 was ferroelectric or non-ferroelectric since data could be obtained only at high temperatures and were not sufficiently sensitive, within experimental errors, to show whether or not a Curie–Weiss temperature dependence was apparent. For more accurate analysis of capacitance data, full
4 equivalent circuit analysis, with the inclusion of constant phase elements to model departures from ideality, would be required and are beyond the scope of this work.

Conductivity data as a function of time at constant temperature are shown in Figs 6a,9a for a selection of temperatures after a bias voltage of 10V [~14.5 Vmm^{-1}] was applied; conductivities rise rapidly at first but gradually level off after sufficiently long times. The difference between initial and final conductivities was at least two orders of magnitude at lower temperatures but decreased with increasing temperature. The initial increase in conductivity occurred more rapidly with increasing temperature and the time required to achieve the final value decreased. Final conductivity values as a function of *dc* bias at constant temperature are shown in Figs 6b,9b. The magnitude of the steady state conductivity increases with *dc* bias, but reaches a limiting value above ~10Vmm^{-1}.

On removing the *dc* bias, conductivity values gradually decreased with time, Figs 6d,9d, and eventually reached steady state values. These steady state values at measuring temperatures < 450 ^{o}C were, however, higher than the initial values before application of the *dc* bias. With increasing temperature, the difference between these steady state and initial values decreased and the initial values could be fully recovered by raising the temperature to e.g. 800 ºC for 1 hour. This shows that there are two excited states which can be separated on removal of the *dc* bias although, on application of the *dc* bias a clear separation of the two excited states is not seen.

Data for R_1 (i.e. σ_1^{-1}) are shown in Arrhenius format in Figs 7a,10a for non-stoichiometric samples that are both TiO_2-deficient and BaO-deficient. The data show linear Arrhenius behaviour of both final and initial conductivities, with and without a *dc* bias. The activation energy decreased significantly with *dc* bias and as a consequence, the conductivity increased by 2-3 orders of magnitude, depending on temperature. Similar effects were seen for R_2 (i.e. σ_2^{-1}), Figs 7b,10b; activation energy data, together with conductivities (R_1^{-1} and R_2^{-1}) at an example temperature, are summarised in Table II.

Confirmation that the conduction mechanism in both sets of non-stoichiometric samples is *p*-type is shown by measurements in different atmospheres, Fig 11. In both cases, the conductivity decreases with decreasing P_{O_2} in the measuring atmosphere; since electrons are injected into the sample as a consequence of desorption of oxygen from the sample surface according to:

$$2O^{2-} \rightarrow O_2 + 4e \qquad (1)$$

This indicates that the injected electrons act to neutralise the *p*-type principal charge carriers.

Discussion

The results presented here on non-stoichiometric BT extend significantly those recently reported for BT ceramics doped with divalent cations,[4-6] Mg^{2+}, Zn^{2+} and Ca^{2+}. The *dc* bias-dependence of the bulk (and grain boundary) conductivity at low bias fields in acceptor-doped and non-stoichiometric BT is, we believe, a novel phenomenon. It is not an effect related to dielectric breakdown at very high voltages; in fact, the characteristics are the opposite of dielectric breakdown since the conductivity increases at small *dc* biases before reaching an essentially constant value with a bias (depending on temperature) of 5-10 Vmm^{-1}. In contrast, high field non-ohmic behaviour has been observed in single crystals of BT and $SrTiO_3$,[9-12] but only above a threshold field of 50 Vmm^{-1}. In the present materials, the *dc* bias dependence was observed at fields as low as 0.7 Vmm^{-1}, although the conductivity changes occur much more slowly at small biases. It is also not associated with charge injection from the electrodes into a conduction band since conduction in both ground and excited states is an activated process.

On removal of the *dc* bias, the conductivities gradually decrease before levelling off at intermediate values. However, the initial (ground state) conductivities are fully recovered after an anneal at e.g. 800 °C. These results on conductivity changes on application, and removal, of a *dc* bias, indicate that significant changes in the electronic structure must occur, with an activation barrier to changes on both application of a *dc* bias and its subsequent removal. The characteristics are therefore quite different to the interface-controlled rapid changes observed with, for instance, ZnO-based varistors. The effect is not associated with the nature of the electrode material (similar effects are seen with both Pt and Au) nor with the atmosphere during measurements (air and N_2). It is not an interface-controlled effect, therefore, such as occurs with Schottky barriers at sample-electrode contacts.

It is not an *ac* effect associated exclusively with local structural changes such as dipole reorientation within defect complexes: impedance data show that the long range conductivity of the samples is affected whereas dipole reorientation is only a local process. It is not associated with a gradient in chemical potential since the samples are chemically homogeneous and there is no evidence of sample decomposition under a *dc* bias. The effect is therefore, an intrinsic property of the materials.

Previously, we have observed similar *dc* bias dependence in three sets of acceptor-doped ceramics, Zn-, Mg and Ca-doped BT,[4-6] in which the divalent acceptor dopants are charge-compensated by the creation of an equal number of oxygen vacancies according to, e.g.:

$$Ti_{Ti}^{x} + O_{O}^{x} \rightarrow Zn_{Ti}^{''} + V_{O}^{\bullet\bullet} \qquad (2)$$

For the present materials, we may consider the nonstoichiometry as arising also from acceptor dopants but in this case, the acceptors are zero-valent cation vacancies, i.e.:

$$Ti_{Ti}^{x} + 2O_{O}^{x} \rightarrow V_{Ti}^{''''} + 2V_{O}^{\bullet\bullet} \qquad (3)$$

or

$$Ba_{Ba}^{x} + O_{O}^{x} \rightarrow V_{Ba}^{''} + V_{O}^{\bullet\bullet} \qquad (4)$$

Consideration of the local defect structure in both acceptor-doped and non-stoichiometric BT indicates large departures from local electroneutrality. The defect structure of TiO_2-deficient BT is shown schematically in Fig 12. It contains a Ti vacancy with two adjacent O vacancies. A large excess negative charge (nominally 4–) is associated with the Ti vacancy; excess positive charge (nominally 2+) is associated with adjacent oxygen vacancies in either *trans* or *cis* (shown) configurations.

Consideration of the large departures from local electroneutrality in the defect complexes leads to a possible mechanism to explain the enhanced conductivity under a *dc* bias. First, it is proposed that the charge polarity is reduced by electron transfer and specifically, by ionisation of electrons from

2*p* orbitals on oxygens adjacent to the cation vacancies. Second, long-range conduction of the resulting holes through the BT lattice occurs. Two electronic defects are created on formation of the excited state, therefore: the ionised electrons which are trapped at sites that, as yet, are unidentified and holes on oxygens adjacent to cation vacancies.

The key to the non-ohmic conductivity appears to be the departure from local electroneutrality in the defect structure. In the case of Mg, Zn, Ca doping, the dopants which substitute for Ti have a nominal net charge 2–. In the TiO_2-deficient sample studied here, we may regard the BT structure as doped with a non-existent, zerovalent ion that has nominal charge 4–.

In the case of BaO-deficient BT, a similar polar defect structure may be proposed that consists of Ba vacancies and associated oxygen vacancies. The Ba vacancies have net charge 2– and the surrounding oxygens may again act as the source of electrons that are ionised, leaving holes on oxygens. The similarity in the Arrhenius plots of the two non-stoichiometric samples indicates a similar conduction mechanism, with and without a *dc* bias, in both cases.

The mechanism by which the electrons are ionised (and subsequently trapped) appears to be one of nucleation and growth which commences at the electrode-sample interface where the relatively small *dc* bias becomes a significantly higher potential gradient; this high potential gradient is responsible for electron ionisation. As a consequence, the *p*-type conductivity rises and the region of high potential gradient gradually moves into the interior of the ceramic, leading to growth in size of excited state domains of higher conductivity. This nucleation and growth mechanism was illustrated in spectroscopic M" plots derived from the experimental impedance data of Mg-doped BT.[5] The initial M" peak associated with the sample grains decreased in size as its volume fraction decreased; a new peak appeared at higher frequency which grew in size as a function of time until it dominated the spectrum and the entire sample was in the excited state.

A characteristic of the materials that show this bulk, low field non-linear effect is that their defect structure has significant departures from local electroneutrality associated with either aliovalent cation doping (Zn^{2+}, Mg^{2+}, Ca^{2+} instead of Ti^{4+}) or charged defect states such as cation vacancies. In all these cases, the oxygens surrounding the defective cation site are underbonded and appear to readily lose an electron via the ionisation process, $O^{2-} \rightarrow O^{-} + e^{-}$. This is consistent with the positive electron affinity[13] for adding a second electron to a gas phase oxygen atom; the resulting O^{2-} ion is stabilised in the solid state only as a consequence of the extra lattice energy associated with doubly-charged oxide ions. Hence, oxide ions surrounding either cation vacancies or substitutional, lower valence cations do not have the same degree of lattice energy stabilisation and may act as a ready source of ionised electrons and holes.

Stoichiometric materials are not expected to show this effect, nor are materials that contain isovalent dopants since these do not lead to departures from local electro-neutrality. Hence, little or no bias dependence is seen for stoichiometric BT or for BT with Ca partially substituting for Ba[6]. It remains to be seen whether any effect is seen with donor dopants, especially those in which cation vacancies are generated via an ionic compensation mechanism. Further studies are in also progress to establish whether this effect is of more general occurrence or is peculiar to $BaTiO_3$.

Finally, it is relevant to consider whether the non-stoichiometric materials studied here may be usefully analysed in terms of Schottky defect equilibria. In stoichiometric $BaTiO_3$, the main intrinsic ionic defects are likely to be Schottky defects involving a combination of cation and anion
5 vacancies. This is because the perovskite structure of BT is unable to accommodate interstitial species of the kind associated with Frenkel defects. In the Schottky defect scenario, a number of cations and anions migrate to the sample surface leaving behind cation and anion vacancies. An equilibrium develops whose equilibrium constant, K, is proportional to the product of the

concentration of anion and cation vacancies. One consequence of aliovalent doping is that, for instance, if the dopant acts to increase the concentration of, say, cation vacancies then this would be compensated by a reduction in the concentration of anion vacancies.

Although such Schottky defect equilibria considerations have often been applied to $BaTiO_3$ ceramics, we believe that they are inappropriate for the present materials. The cation and anion vacancies generated in the non-stoichiometric samples occur as a consequence of compositional change and not from intrinsic Schottky defect formation. Thus, in the TiO_2-deficient samples the local defect structure must contain two oxygen vacancies for every Ti vacancy; their relative concentrations are not constrained by the Schottky equilibrium constant, K; instead, their relative concentrations depend only on the overall composition. Similarly, for BaO-deficient samples there must be equal numbers of Ba and oxygen vacancies whose actual number is given by the overall sample composition. Whilst, Schottky equilibria considerations do provide a useful starting point in considering the defect structures of BT, they are limited to dilute, point defect structures in which K is unaffected by dopants or stoichiometry changes. In the present materials, the solid solution thermodynamics are clearly not controlled by Schottky defect equilibria.

Conclusions

The electrical properties of BaO-deficient and TiO_2-deficient BT (non-stoichiometric-BT) are very different from those of stoichiometric BT. The conductivity of stoichiometric-BT is insensitive to the application of a small *dc* bias in the range ~ 0.5 to 20 Vmm^{-1} for temperatures up to at least 700 ^{o}C. By contrast, the conductivity (both bulk and grain boundary) of non-stoichiometric-BT increases with a *dc* bias. The increase is time- and temperature-dependent and is reversible on removal of the *dc* bias.

The defect structure of non-stoichiometric-BT is not known in detail but probably consists of cation vacancies together with the required number of adjacent oxygen vacancies to achieve charge balance. The resulting defect structure is highly polar with negatively charged cation vacancies and positively charged oxygen vacancies. It is proposed that the polarity may be reduced by electron transfer leading to creation of a more conductive exited state. The source of the electrons is likely to be underbonded oxide ions surrounding the cation vacancies.

Non-linear low field bulk resistivity is not a phenomenon that is usually found, or expected, with moderately resistive materials that conduct by a mechanism of ion or electron hopping. Its occurrence in both nonstoichiometric and Mg, Zn, Ca-doped BT, but not in undoped, stoichiometric BT, is believed to be a consequence of the acceptor doping mechanism [i.e. doping with lower valence cation and associated creation of oxygen vacancies]; in the case of non-stoichiometric-BT, the mechanism is the same because the acceptor dopants are, effectively, the zero-valent cation vacancies.

The electrical properties of BaO-deficient and TiO_2-deficient BT are similar. This indicates that the electron transfer mechanism within the BT defect structure is more important than the nature of the acceptor dopant (V_{Ba}'' or V_{Ti}''''). Since underbonded oxygens appear to be the critical component of the defect structure that are responsible for the non-linearity, similar effects may be anticipated with other ceramic materials containing acceptor dopants which have an oxygen vacancy charge compensation mechanism.

Evidence for non-stoichiometry in $BaTiO_3$ is obtained from T_C data of both BaO- and TiO_2-deficient samples, which are consistently a few degrees lower than that of stoichiometric $BaTiO_3$. This is supported by the observed non-linear phenomena for which non-stoichiometry appears to be a necessary pre-requisite.

Acknowledgments

ARW thanks the EPSRC for financial support. MP, HB, EC thank the “Bancaja-Universitat Jaume I”- project No. P1 1B2006-25 for financial support and the Generalitat Valenciana for a fellowship BFPI/2007/174 for MP.

References

[1] A. J. Moulson and J. M. Herbert, *Electroceramics*, Second Edition, Wiley, 2003.

[2] R. A. Huggins, *Diffusion in Solids, Recent Development*. Edited by A. S. Nowick and J. J. Burton, Academic Press, 1975.

[3] D. B. Strukov, G. S. Snider, D. R Stewart, and R. S Williams, “The Missing Memristor Found”, *Nature,* 2008, **453**, 80.

[4] H. Beltrán, M. Prades, N. Masó, E. Cordoncillo, and A. R. West,” Voltage-Dependent Low-Field Bulk Resistivity in $BaTiO_3$:Zn Ceramics”, *J. Am. Ceram. Soc.*, **93[2]**, 500–505 (2010).

[5] M. Prades, N. Masó, H. Beltrán, E. Cordoncillo, and A. R. West, “Field enhanced bulk conductivity of $BaTiO_3$: Mg ceramics”, *J. Mater. Chem.*, **20[25]**, 5335–5344, (2010).

[6] N. Masó, M. Prades, H. Beltrán, E. Cordoncillo, D. C. Sinclair and A. R. West, “Field enhanced bulk conductivity of acceptor-doped $BaTi_{1-x}Ca_xO_{3-x}$ ceramics”, *Appl. Phys. Lett.*, **97[6]**, 062907 (2010).

[7] H. Beltrán, E. Cordoncillo, P. Escribano, D. C. Sinclair, and A. R. West, “Insulating properties of lanthanum-doped $BaTiO_3$ ceramics prepared by low-temperature synthesis”, *J. Am. Ceram. Soc.*, **87[11]**, 2132–2134 (2004).

[8] J.T.S. Irvine, D.C. Sinclair, and A.R. West, “Electroceramics: Characterization by impedance spectroscopy”, *Adv. Mater.*, **2[3]** 132–138 (1990).

[9] A. Branwood and R.H. Tredgold, "The electrical conductivity of barium titanate single crystals", *Proc. Phys. Soc.*, **76[1]** 93–98 (1960).

[10] A. Branwood, O.H. Hughes, J.D. Hurd and R.H. Tredgold, "Evidence for space charge conduction in barium titanate single crystals", *Proc. Phys. Soc.*, **79[6]** 1161– 1165 (1962).

[11] G.A. Cox and R.H. Tredgold, "Double space charge injection in solids", *Phys. Letters*, **4[3]** 199–200 (1963).

[12] G.A. Cox and R.H. Tredgold, "Time dependence of the electrical conductivity in strontium titanate single crystals", *Brit. J. Appl. Phys.*, **16[4]** 427–430 (1965).

[13] C. A. McDowell, *Physical Chemistry*, Edited by H. Eyring, D. Henderson and W. Jost, Vol. 3, Academic Press, 1969.

Table Caption

Table I. Pellet density, D_r (%), lattice parameters (in Å), grain size (in μm), T_C, T_0, T_C–T_0 and C_W (in °C) for all samples sintered at 1400 °C. Estimated errors in T_C and T_0 are ~1 and 2 °C, respectively.

Table II. Conductivity values obtained at 400 °C, by interpolation/extrapolation, and activation energy of R_1 and R_2 components for all samples sintered at 1400 °C.

Table I. Pellet density, D_r (%), lattice parameters (in Å), grain size (in μm), T_C, T_0, T_C–T_0 and C_W (in °C) for all samples sintered at 1400 °C. Estimated errors in T_C and T_0 are ~1 and 2 °C, respectively.

		D_r	lattice parameters		grain size	T_C	T_0	T_C–T_0	C_W
			a	*c*					
Sol-gel	$BaTi_{0.99}O_{2.98}$	83	3.9893(8)	4.0329(13)	15–150	129	113	16	68000
	$Ba_{0.99}TiO_{2.99}$	82	3.9899(10)	4.0321(16)	15–150	128	117	11	87000
	$BaTiO_3$	87	3.9953(2)	4.0313(3)	15–150	135	125	10	128000
Solid state	$BaTi_{0.99}O_{2.98}$	98	3.9963(3)	4.0362(4)	1–3	129	79	50	130000
	$Ba_{0.99}TiO_{2.99}$	94	3.9947(2)	4.0352(3)	15–150	130	120	10	124000
	$BaTiO_3$	90	3.9966(6)	4.0357(9)	15–50	133	123	10	124000

Table II. Conductivity values obtained at 400 ºC, by interpolation/extrapolation, and activation energy of R_1 and R_2 components for all samples sintered at 1400 ºC.

				$BaTi_{0.99}O_{2.98}$	$Ba_{0.99}TiO_{2.99}$	$BaTiO_3$
Sol-gel	R_1	Ea /eV	0V	1.30(4)	1.34(5)	0.71(1)
			10V	0.80(1)	0.82(1)	-
		σ /Scm^{-1}	0V	$4.22x10^{-6}$	$7.09x10^{-6}$	$6.39x10^{-5}$
			10V	$6.03x10^{-4}$	$5.39x10^{-4}$	-
	R_2	Ea /eV	0V	1.28(3)	1.30(2)	1.49(2)
			10V	0.72(1)	0.77(1)	-
		σ /Scm^{-1}	0V	$5.21x10^{-7}$	$1.62x10^{-6}$	$2.38x10^{-7}$
			10V	$3.31x10^{-5}$	$4.97x10^{-5}$	-
Solid state	R_1	Ea /eV	0V	1.08(4)	1.18(3)	1.15(4)
			10V	0.76(3)	1.24(6)	1.05(4)
		σ /Scm^{-1}	0V	$5.89x10^{-6}$	$2.61x10^{-6}$	$1.36x10^{-6}$
			10V	$4.08x10^{-5}$	$3.74x10^{-5}$	$2.51x10^{-6}$
	R_2	Ea /eV	0V	-	1.59(5)	1.24(4)
			10V	-	1.11(3)	1.25(4)
		σ /Scm^{-1}	0V	-	$7.79x10^{-7}$	$6.10x10^{-7}$
			10V	-	$1.10x10^{-5}$	$7.34x10^{-7}$

Figure Captions

Fig 1. SEM of the pellet surface sintered at 1400 ºC of $BaTiO_3$, $Ba_{0.99}TiO_{2.98}$ and $BaTi_{0.99}O_{2.98}$ prepared by sol-gel (a, c and e, respectively) and solid state reaction (b, d and f, respectively). Scale bars: a, b, d: 10μm; c, e: 100μm; f: 3μm.

Fig 2. Permittivity data $\varepsilon_r^{'}$ and Curie-Weiss plot at 100 kHz as a function of temperature for $BaTi_{0.99}O_{2.98}$ (■), $Ba_{0.99}TiO_{2.99}$ (○), and $BaTiO_3$ (▲) prepared by sol-gel (a,c) and (b,d) solid state reaction at 1400ºC. Estimated errors in T_C and T_0 are ~1 and 2 °C, respectively.

Fig 3. Impedance complex plane plots, M" spectroscopic plots and capacitance data at 472ºC for stoichiometric $BaTiO_3$ prepared by sol-gel (a, b, c) and solid state reaction (d, e, f), before and after a voltage of 10V [6.7 and 7.1 Vmm^{-1}, respectively] was applied.

Fig 4. Arrhenius plots of (a) σ_1 and (b) σ_2 for stoichiometric $BaTiO_3$ measured without a *dc* bias and with an applied voltage of 10V [6.7 and 7.1 Vmm^{-1} for solid state and sol-gel samples, respectively] after a steady state had been reached. Activation energies in eV, with errors in the range 0.02–0.05 eV, are shown beside each data set.

Fig 5. Impedance complex plane plots, M" spectroscopic plots and capacitance data at 485ºC and 477ºC for $BaTi_{0.99}O_{2.98}$ prepared by sol-gel (a, b, c) and solid state reaction (d, e, f), before and after a voltage of 10V [15.1 and 9.52 Vmm^{-1}, respectively] was applied. Note: for the sample prepared by solid state reaction, there is no evidence for a separate grain boundary resistance R_2.

Fig 6. $BaTi_{0.99}O_{2.98}$, sol-gel sample: (a) Bulk conductivity, σ_1, at different temperatures *vs* time after a voltage 10V [15.1 Vmm^{-1}] was applied; (b) σ_1 *vs* time for different applied voltages at constant temperature, 335 ^{o}C; (c) limiting bulk conductivity *vs* bias voltage measured at 335 ºC; and (d) σ_1 at different measuring times after removal of the *dc* bias measured at 385 ºC, 432 ºC and 482ºC (lines indicate the ground state for each temperature).

Fig 7. Arrhenius plots of (a) σ_1 and (b) σ_2 for $BaTi_{0.99}O_{2.98}$ measured without a *dc* bias and with an applied voltage of 10V [9.52 and 15.1 Vmm^{-1} for solid state and sol-gel samples, respectively] after a steady state had been reached. Activation energies in eV, with errors in the range 0.02–0.05 eV, are shown beside each data set.

Fig 8. Impedance complex plane plots, M" spectroscopic plots and capacitance data at 469ºC and 475ºC for $Ba_{0.99}TiO_{2.99}$ prepared by sol-gel (a, b, c) and solid state reaction (d, e, f), before and after a voltage of 10V [13.7 and 8.7 Vmm^{-1}, respectively] was applied.

Fig 9. $Ba_{0.99}TiO_{2.99}$, sol-gel sample: (a) Bulk conductivity, σ_1, at different temperatures *vs* time after a voltage 10V [13.7 Vmm^{-1}] was applied; (b) σ_1 *vs* time for different applied voltages at constant temperature, 306 ^{o}C; (c) limiting bulk conductivity *vs* bias voltage measured at 306 ºC; and (d) σ_1 at different measuring times after removal of the *dc* bias measured at 386 ºC, 431 ºC and 486ºC (lines indicate the ground state for each temperature).

Fig 10. Arrhenius plots of (a) σ_1 and (b) σ_2 for $Ba_{0.99}TiO_{2.99}$ measured without a *dc* bias and with an applied voltage of 10V [8.7 and 13.7 Vmm^{-1} for solid state and sol-gel samples, respectively] after a steady state had been reached. Activation energies in eV, with errors in the range 0.02–0.05 eV, are shown beside each data set.

Fig 11. Impedance complex plane plots in different measuring atmospheres for (a) $BaTi_{0.99}O_{2.98}$ and (b) $Ba_{0.99}TiO_{2.99}$ prepared by solid state reaction.

Fig 12. Idealised defect structure for non-stoichiometric $BaTiO_3$ with titanium and oxygen vacancies. The oxygen vacancies are shown *cis* but could also be *trans*.

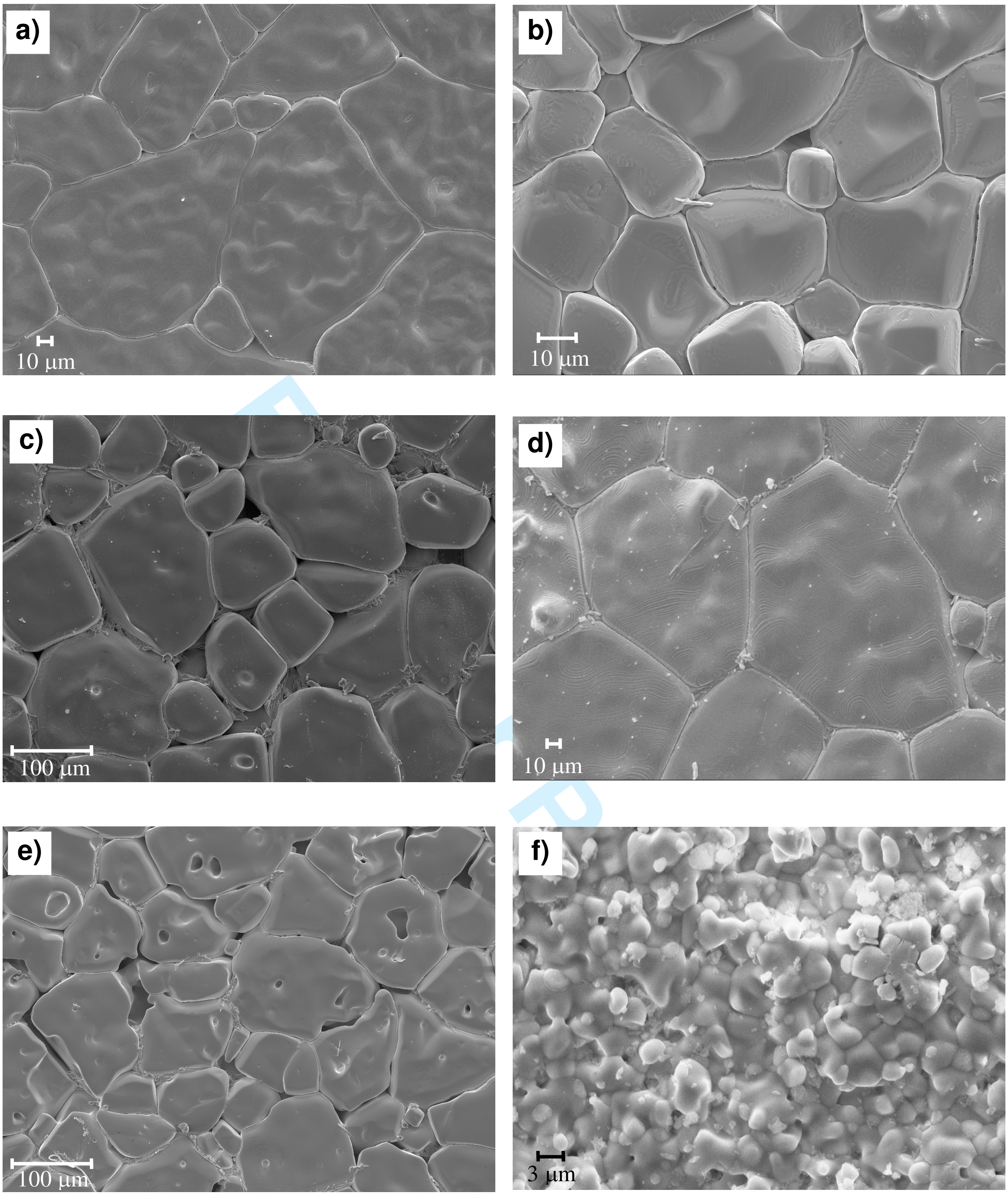

Fig 1. SEM of the pellet surface sintered at 1400 ºC of $BaTiO_3$, $Ba_{0.99}TiO_{2.98}$ and $BaTi_{0.99}O_{2.98}$ prepared by sol-gel (a, c and e, respectively) and solid state reaction (b, d and f, respectively). Scale bars: a, b, d: 10µm; c, e: 100µm; f: 3µm.

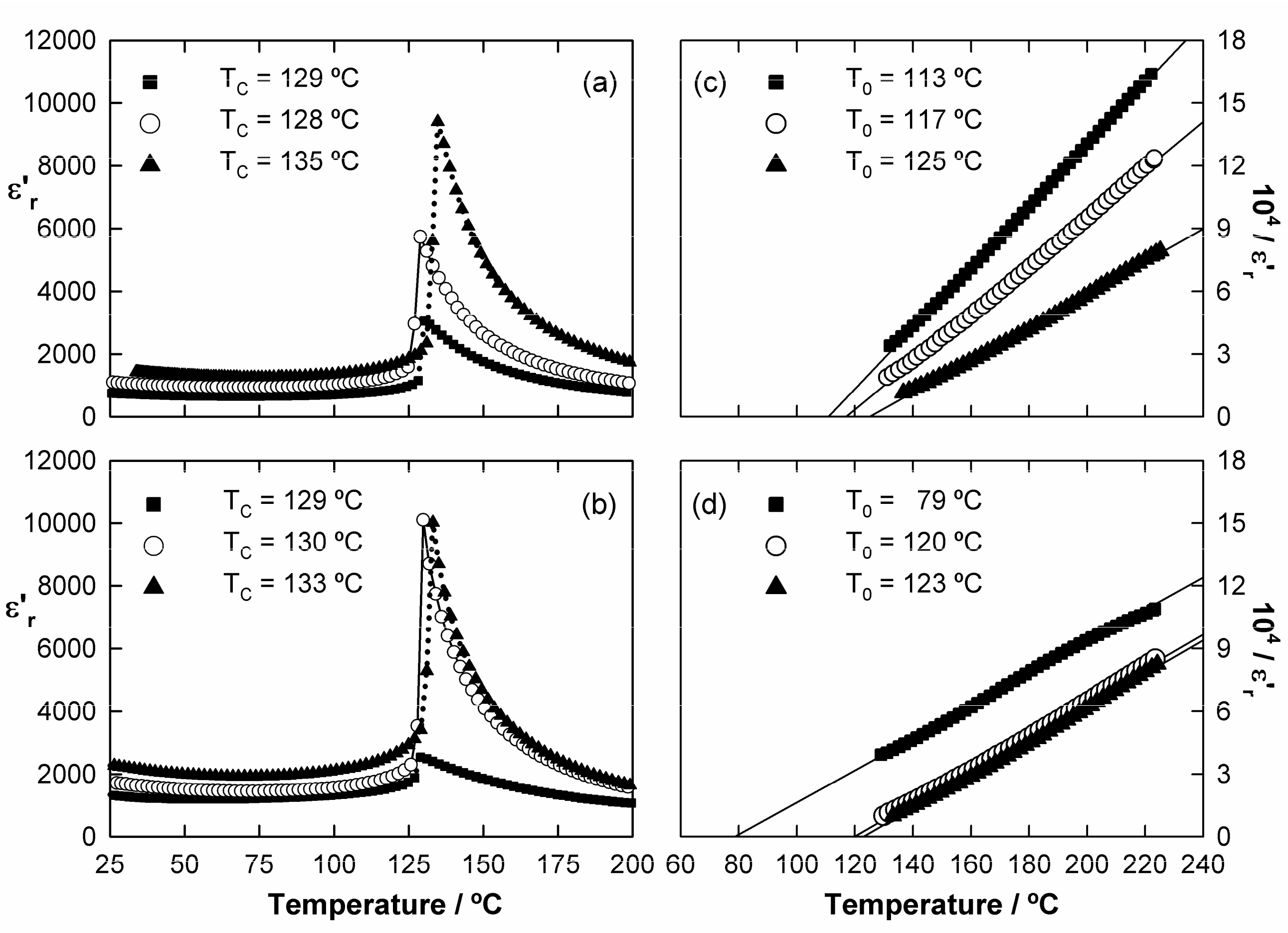

Fig 2. Permittivity data $\varepsilon_r^{'}$ and Curie-Weiss plot at 100 kHz as a function of temperature for $BaTi_{0.99}O_{2.98}$ (■), $Ba_{0.99}TiO_{2.99}$ (○), and $BaTiO_3$ (▲) prepared by sol-gel (a,c) and (b,d) solid state reaction at 1400ºC. Estimated errors in T_C and T_0 are ~1 and 2 ^oC, respectively.

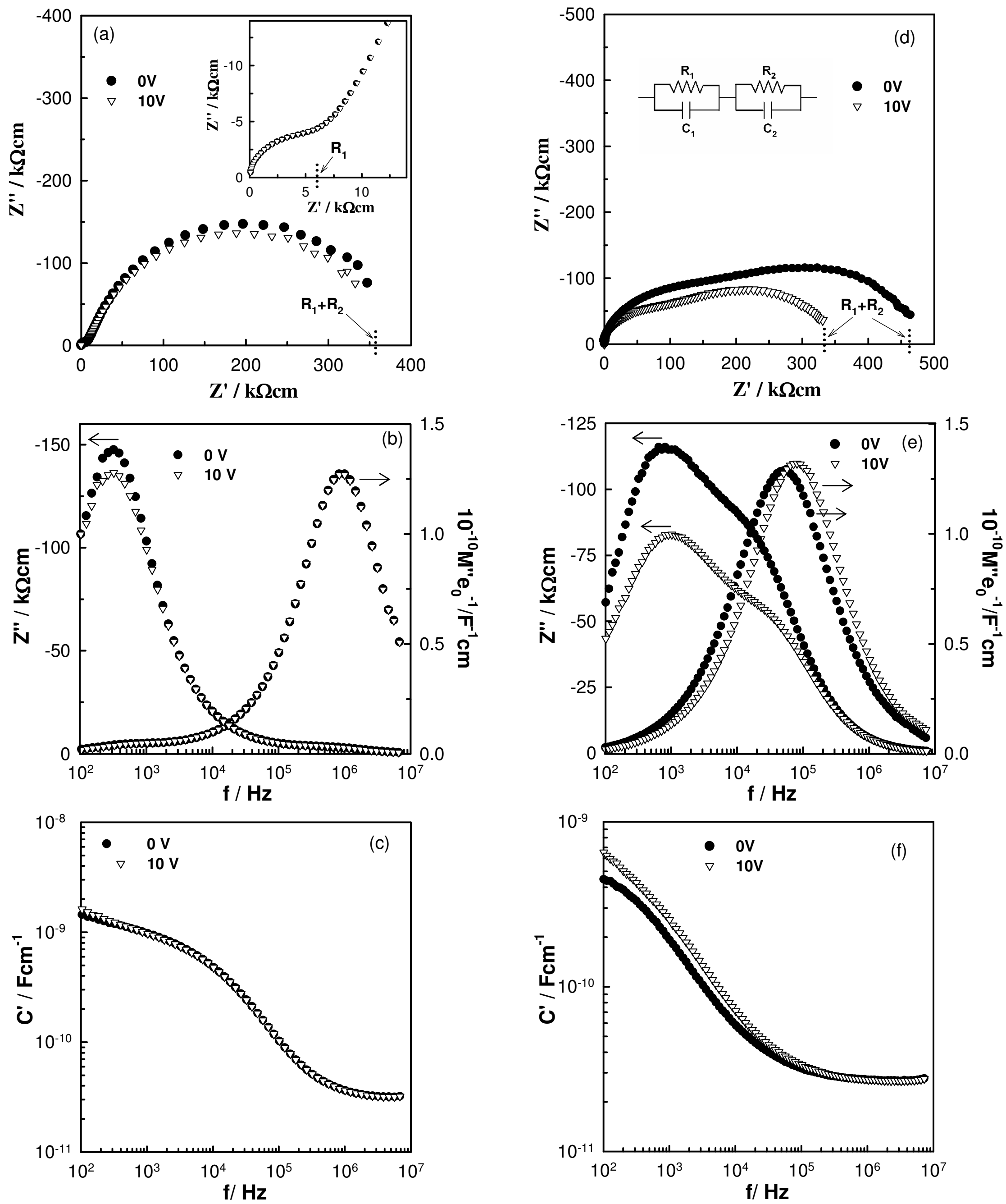

Fig 3. Impedance complex plane plots, M" spectroscopic plots and capacitance data at 472ºC for stoichiometric $BaTiO_3$ prepared by sol-gel (a, b, c) and solid state reaction (d, e, f), before and after a voltage of 10V [6.7 and 7.1 Vmm^{-1}, respectively] was applied.

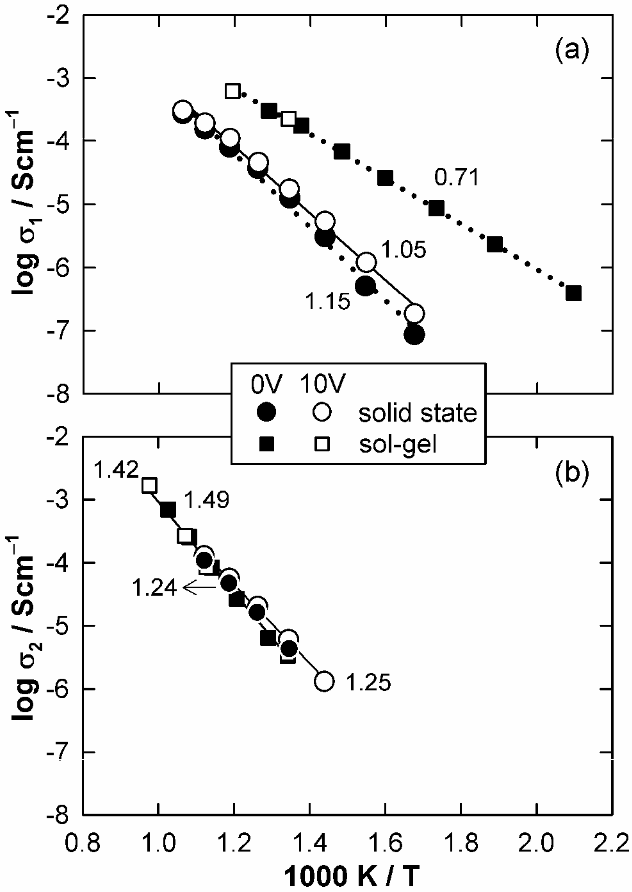

Fig 4. Arrhenius plots of (a) σ_1 and (b) σ_2 for stoichiometric $BaTiO_3$ measured without a *dc* bias and with an applied voltage of 10V [6.7 and 7.1 Vmm^{-1} for solid state and sol-gel samples, respectively] after a steady state had been reached. Activation energies in eV, with errors in the range 0.01–0.05 eV, are shown beside each data set.

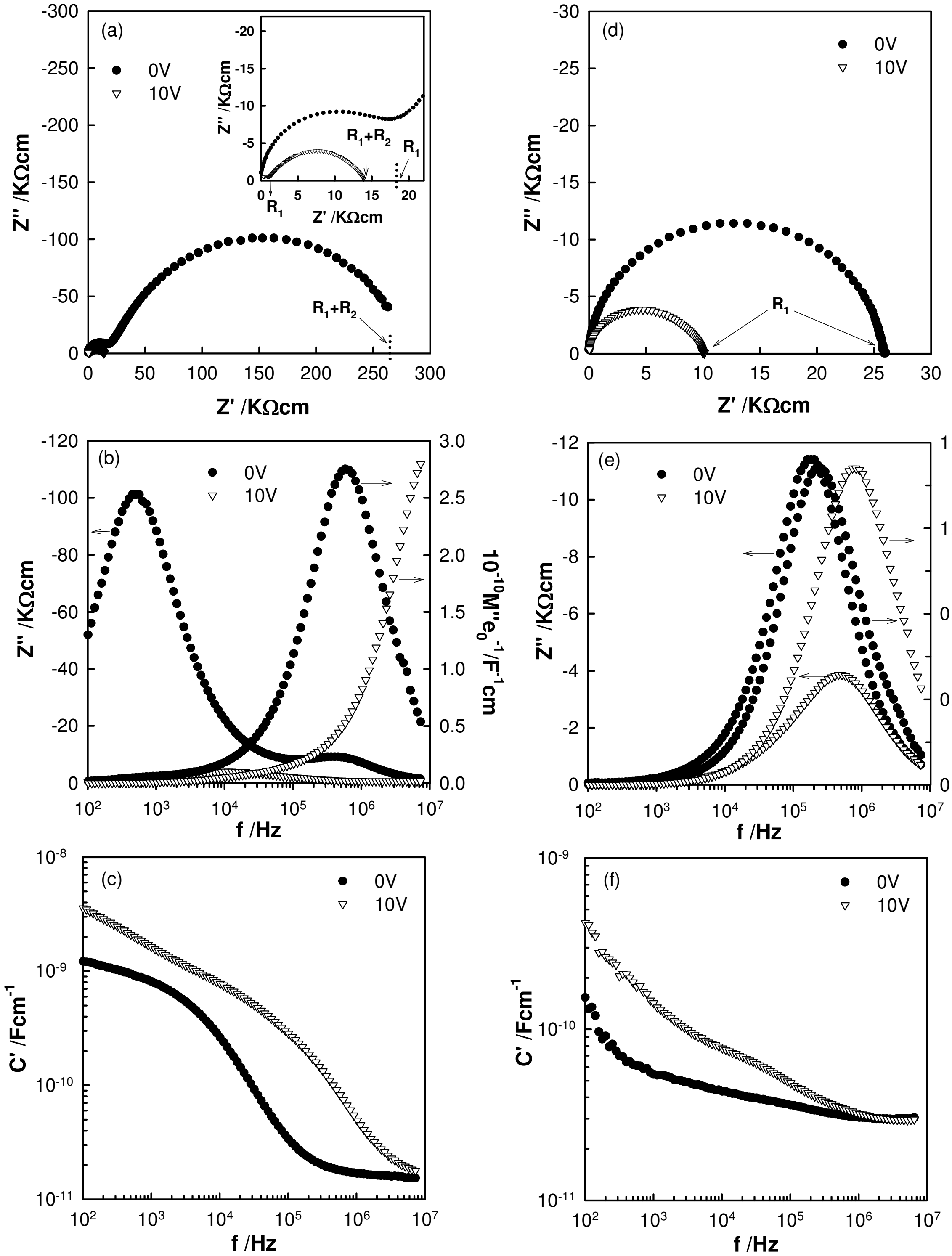

Fig 5. Impedance complex plane plots, M" spectroscopic plots and capacitance data at 485ºC and 477ºC for $BaTi_{0.99}O_{2.98}$ prepared by sol-gel (a, b, c) and solid state reaction (d, e, f), before and after a voltage of 10V [15.1 and 9.52 Vmm^{-1}, respectively] was applied. Note: for the sample prepared by solid state reaction, there is no evidence for a separate grain boundary resistance R_2.

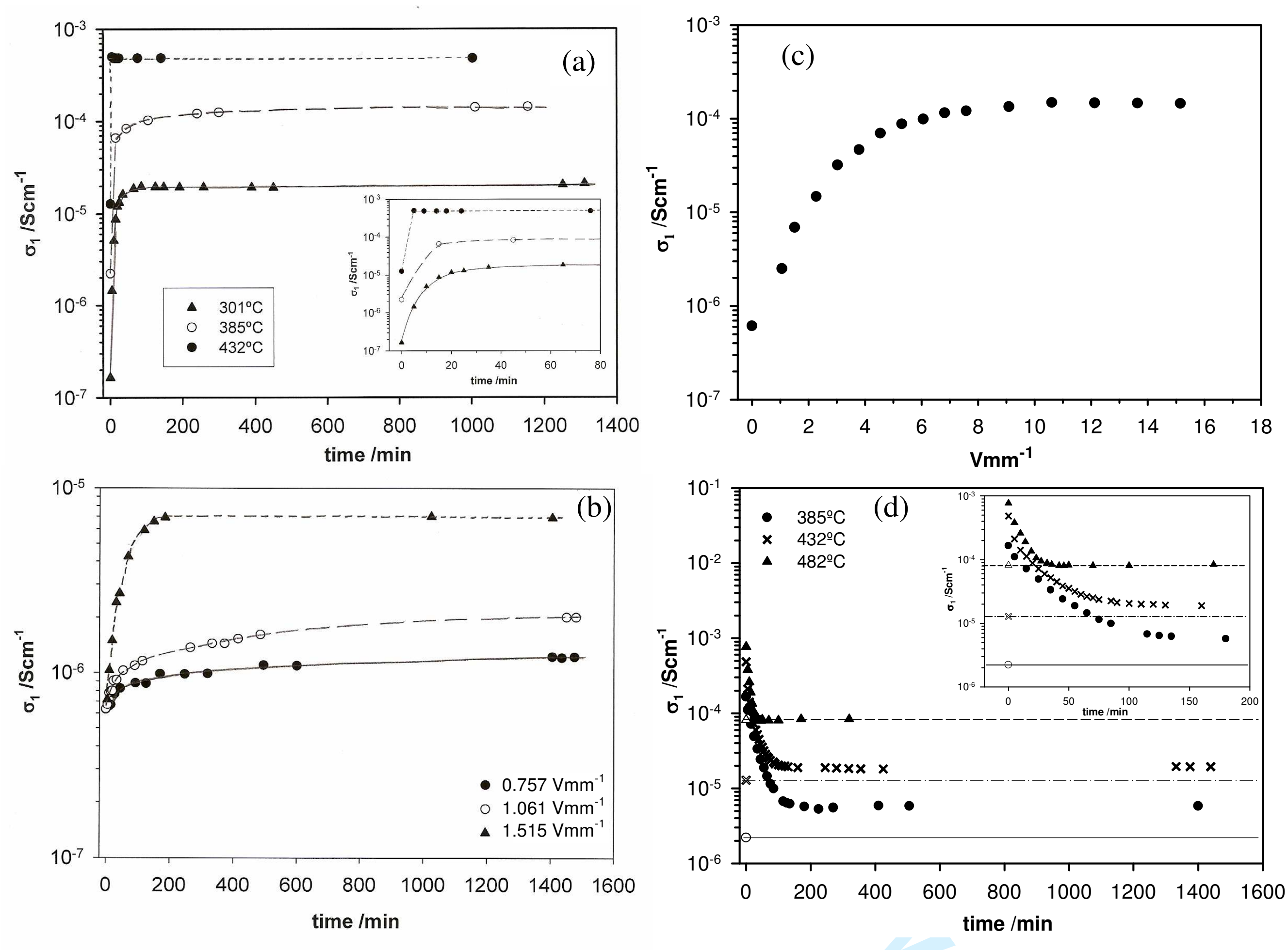

Fig 6. BaTi$_{0.99}$O$_{2.98}$, sol-gel sample: (a) Bulk conductivity, σ_1, at different temperatures *vs* time after a voltage 10V [15.1 Vmm^{-1}] was applied; (b) σ_1 *vs* time for different applied voltages at constant temperature, 335 ^{o}C; (c) limiting bulk conductivity *vs* bias voltage measured at 335 ºC; and (d) σ_1 at different measuring times after removal of the *dc* bias measured at 385 ºC, 432 ºC and 482ºC (lines indicate the ground state for each temperature).

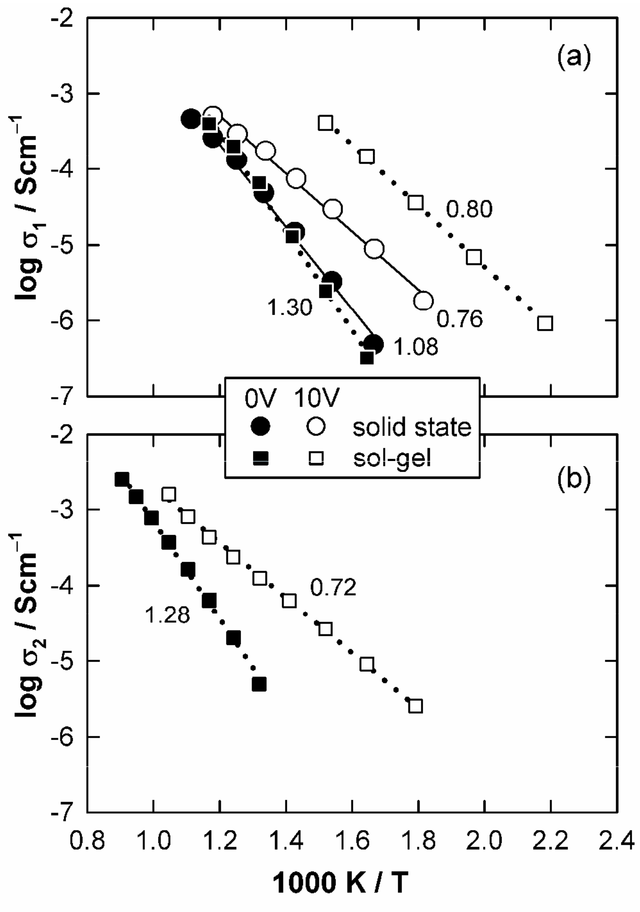

Fig 7. Arrhenius plots of (a) σ_1 and (b) σ_2 for $BaTi_{0.99}O_{2.98}$ measured without a *dc* bias and with an applied voltage of 10V [9.52 and 15.1 Vmm^{-1} for solid state and sol-gel samples, respectively] after a steady state had been reached. Activation energies in eV, with errors in the range 0.01–0.05 eV, are shown beside each data set.

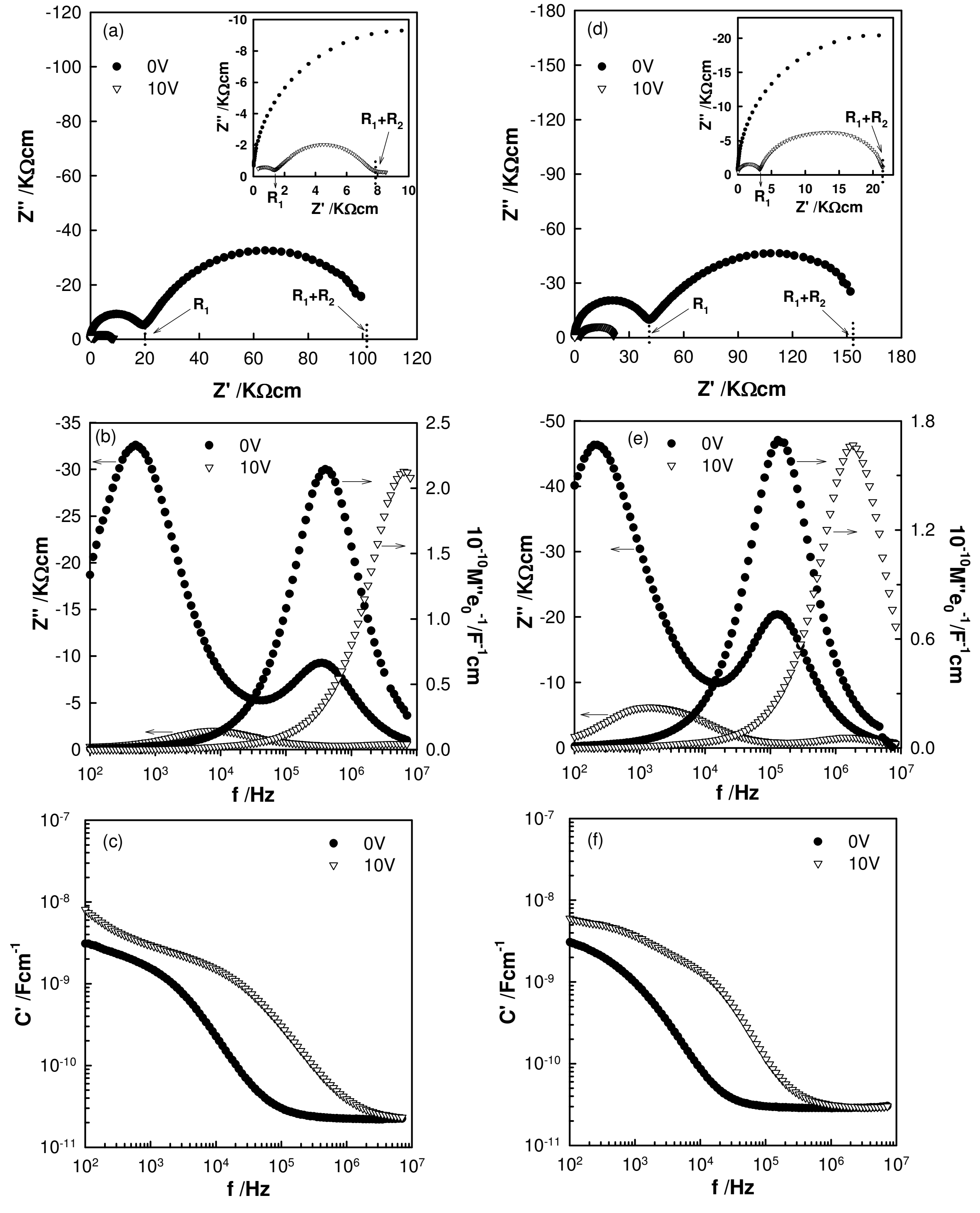

Fig 8. Impedance complex plane plots, M” spectroscopic plots and capacitance data at 469ºC and 475ºC for $Ba_{0.99}TiO_{2.99}$ prepared by sol-gel (a, b, c) and solid state reaction (d, e, f), before and after a voltage of 10V [13.7 and 8.7 Vmm^{-1}, respectively] was applied.

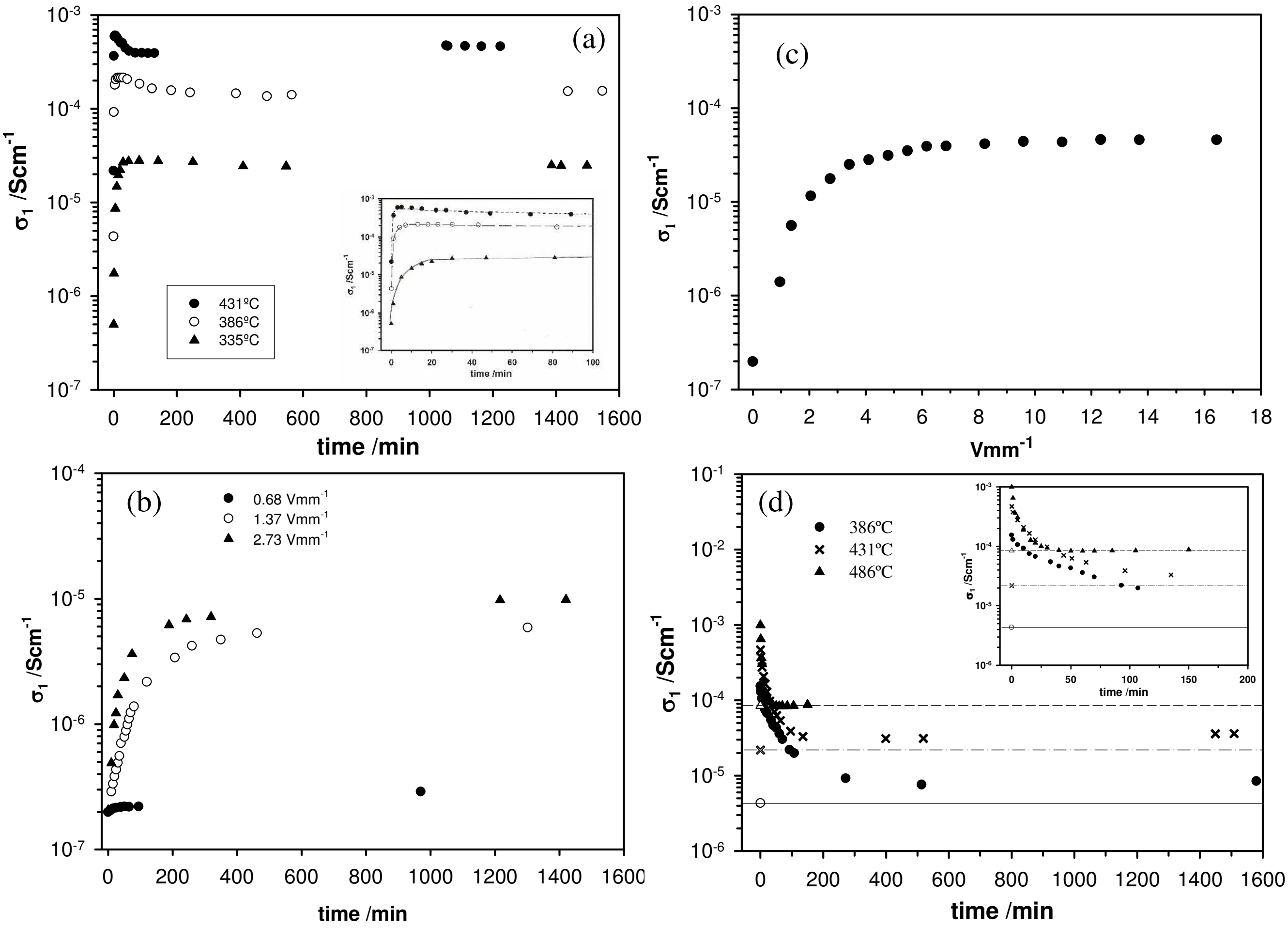

Fig 9. $Ba_{0.99}TiO_{2.99}$, sol-gel sample: (a) Bulk conductivity, σ_1, at different temperatures *vs* time after a voltage 10V [13.7 Vmm^{-1}] was applied; (b) σ_1 *vs* time for different applied voltages at constant temperature, 306 °C; (c) limiting bulk conductivity *vs* bias voltage measured at 306 ºC; and (d) σ_1 at different measuring times after removal of the *dc* bias measured at 386 ºC, 431 ºC and 486ºC (lines indicate the ground state for each temperature).

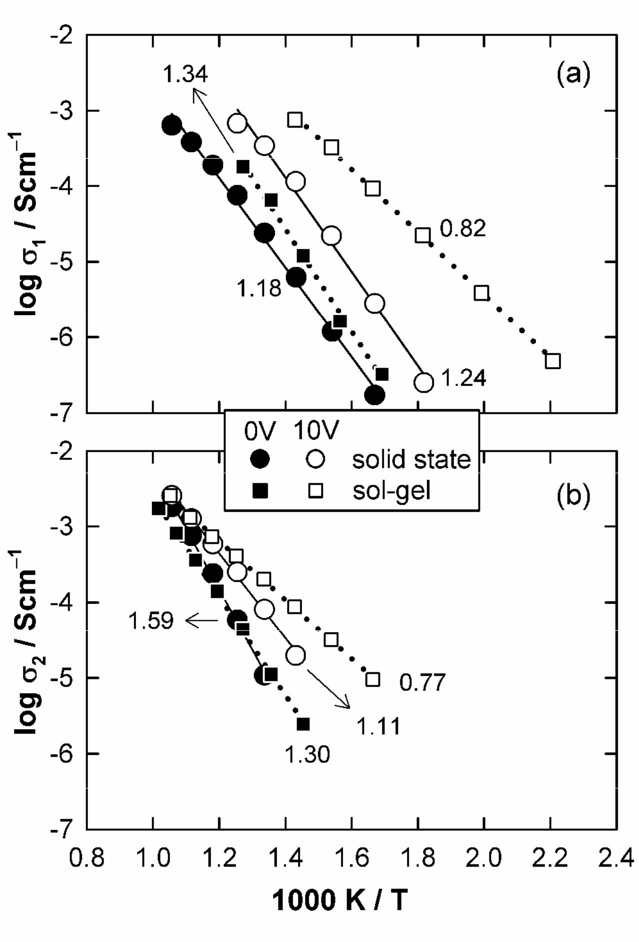

Fig 10. Arrhenius plots of (a) σ_1 and (b) σ_2 for $Ba_{0.99}TiO_{2.99}$ measured without a *dc* bias and with an applied voltage of 10V [8.7 and 13.7 Vmm^{-1} for solid state and sol-gel samples, respectively] after a steady state had been reached. Activation energies in eV, with errors in the range 0.01–0.05 eV, are shown beside each data set.

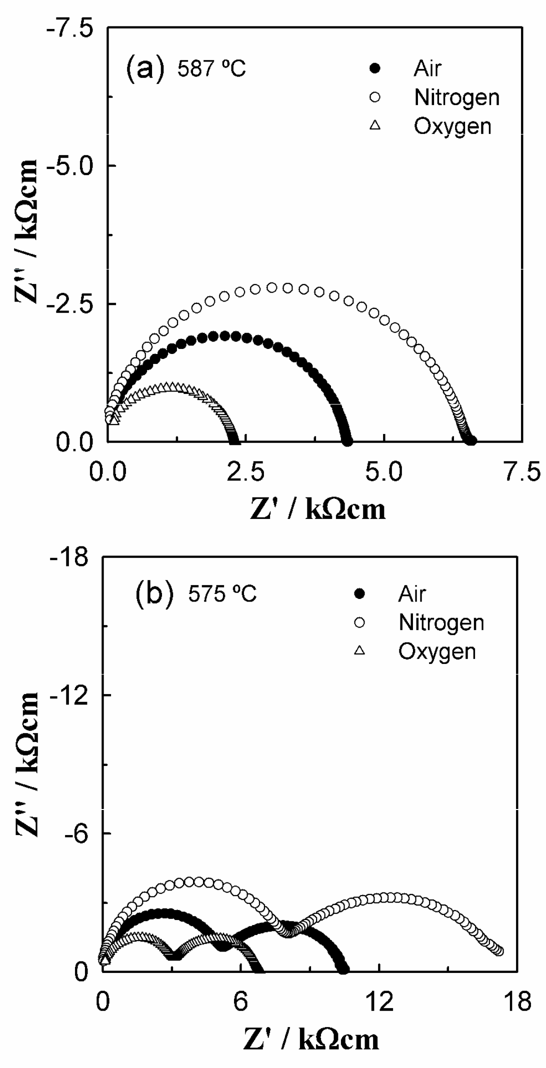

Fig 11. Impedance complex plane plots in different measuring atmospheres for (a) $BaTi_{0.99}O_{2.98}$ and (b) $Ba_{0.99}TiO_{2.99}$ prepared by solid state reaction.

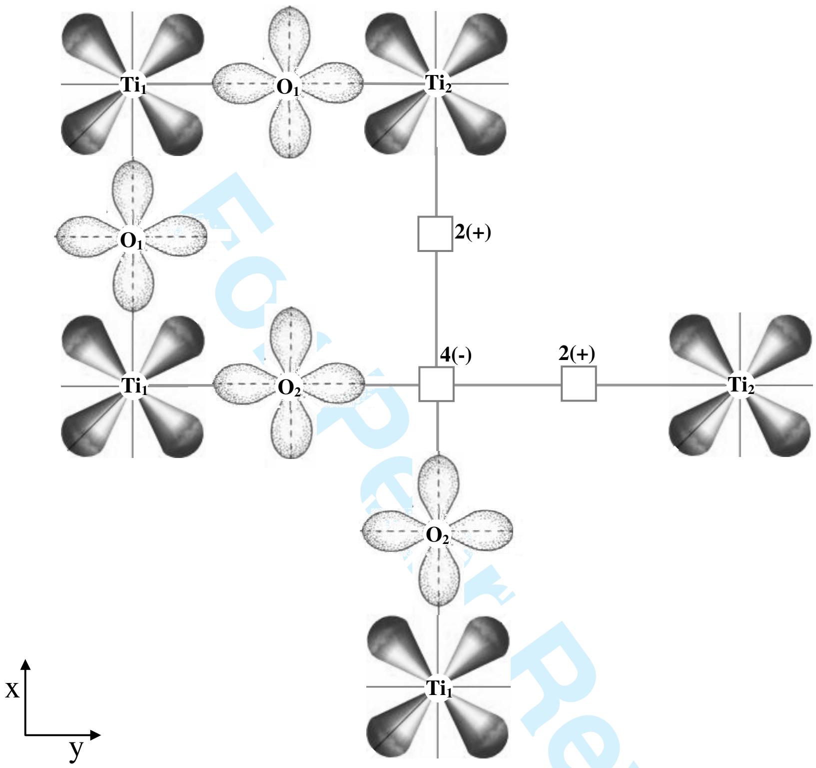

Fig 12. Idealised defect structure for non-stoichiometric $BaTiO_3$ with titanium and oxygen vacancies. The oxygen vacancies are shown *cis* but could also be *trans*.

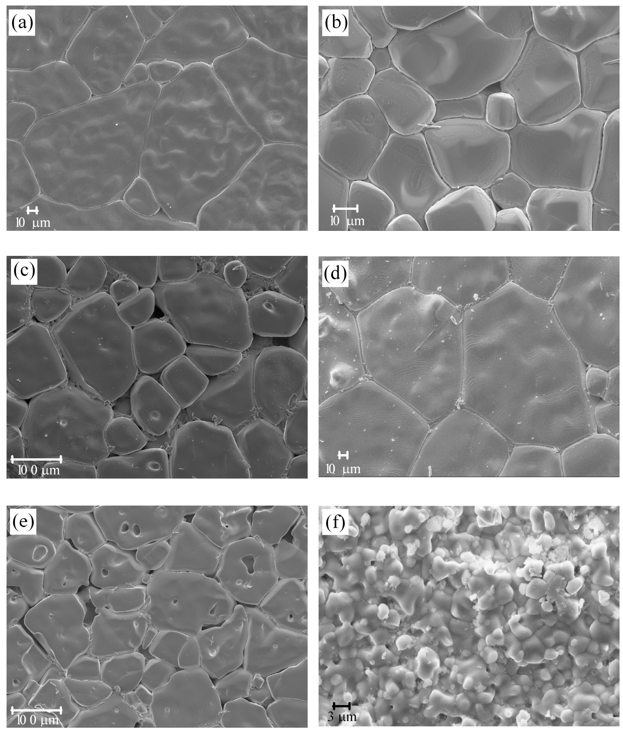

671x1187mm (150 x 150 DPI)

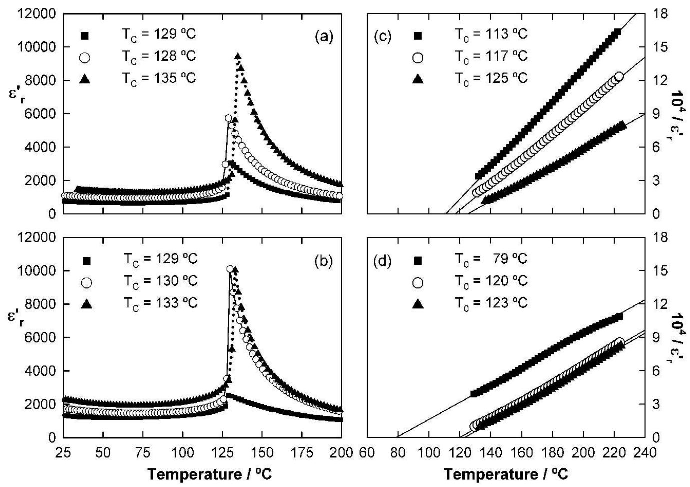

679x1187mm (150 x 150 DPI)

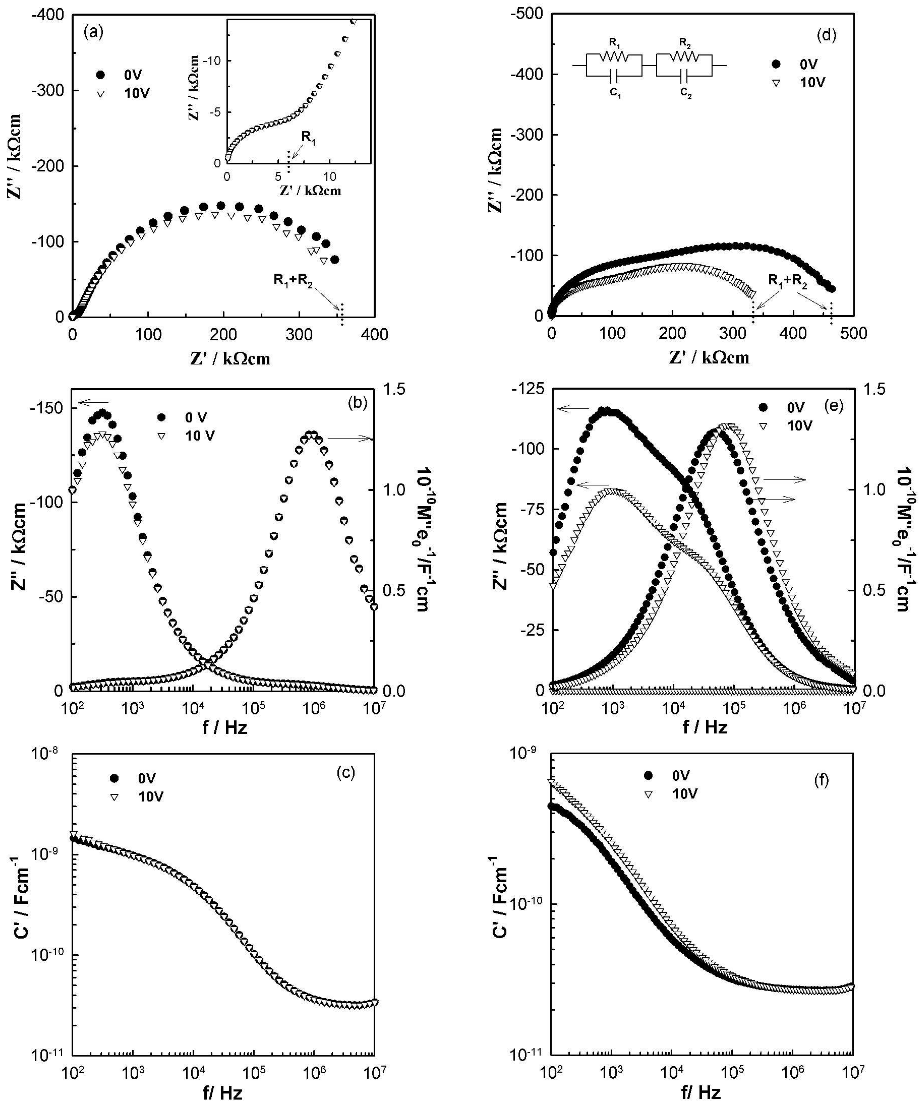

671x789mm (150 x 150 DPI)

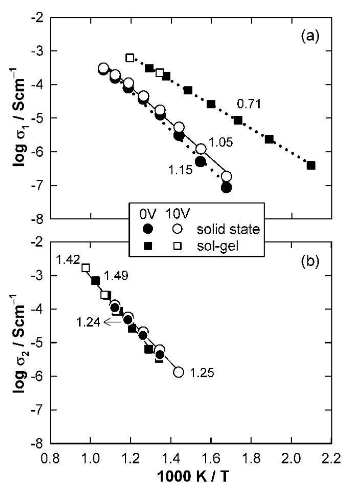

339x1187mm (150 x 150 DPI)

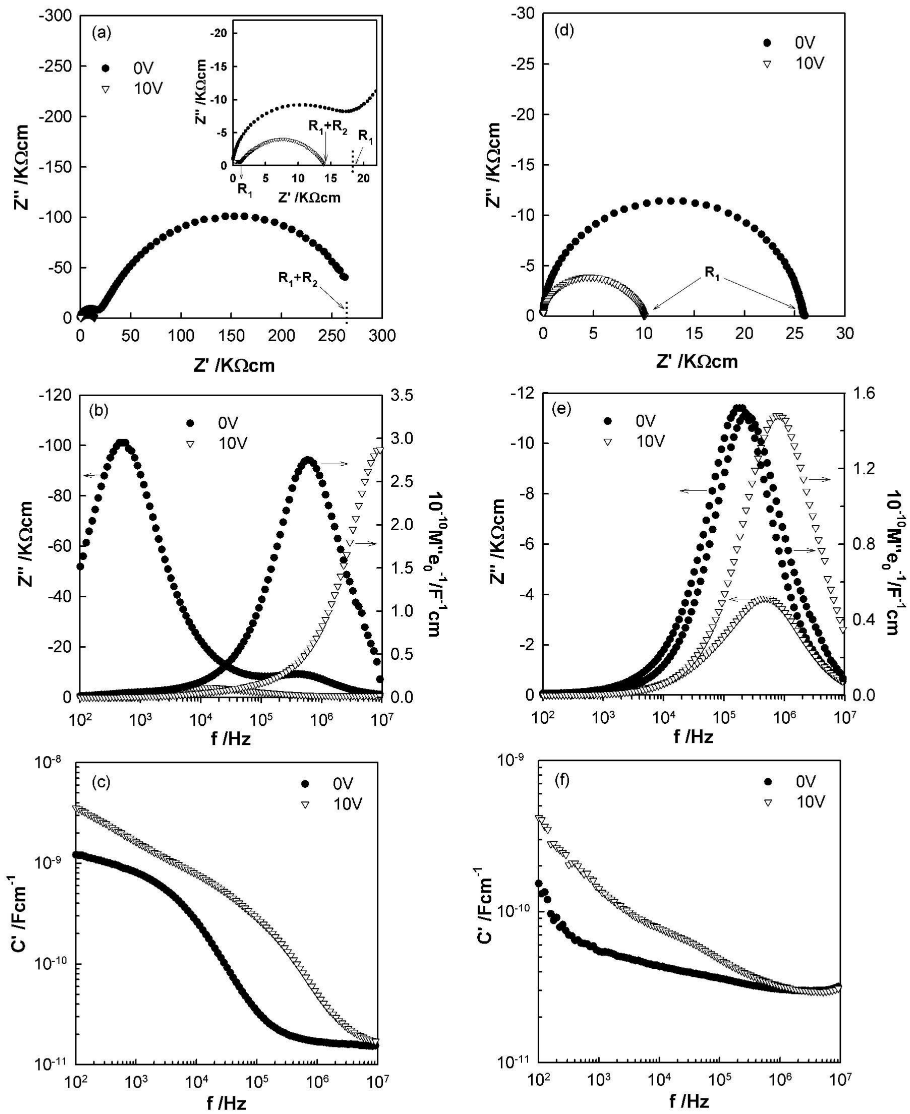

671x789mm (150 x 150 DPI)

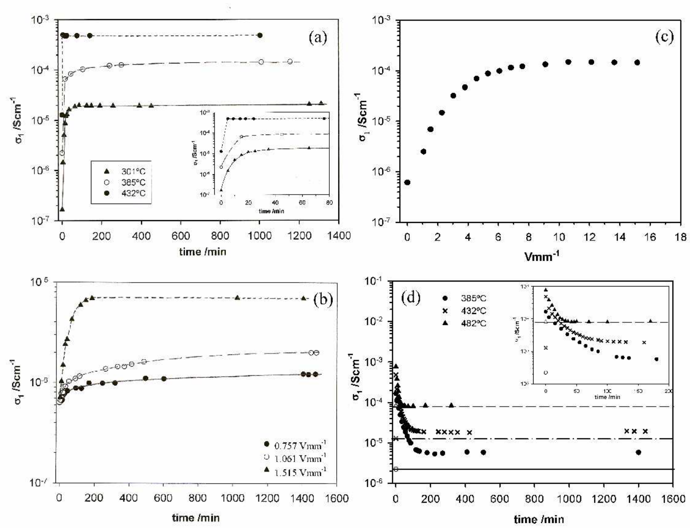

671x997mm (150 x 150 DPI)

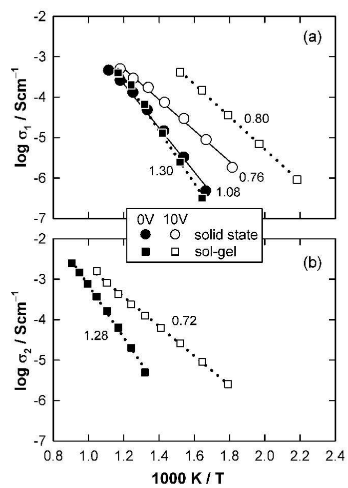

339x1187mm (150 x 150 DPI)

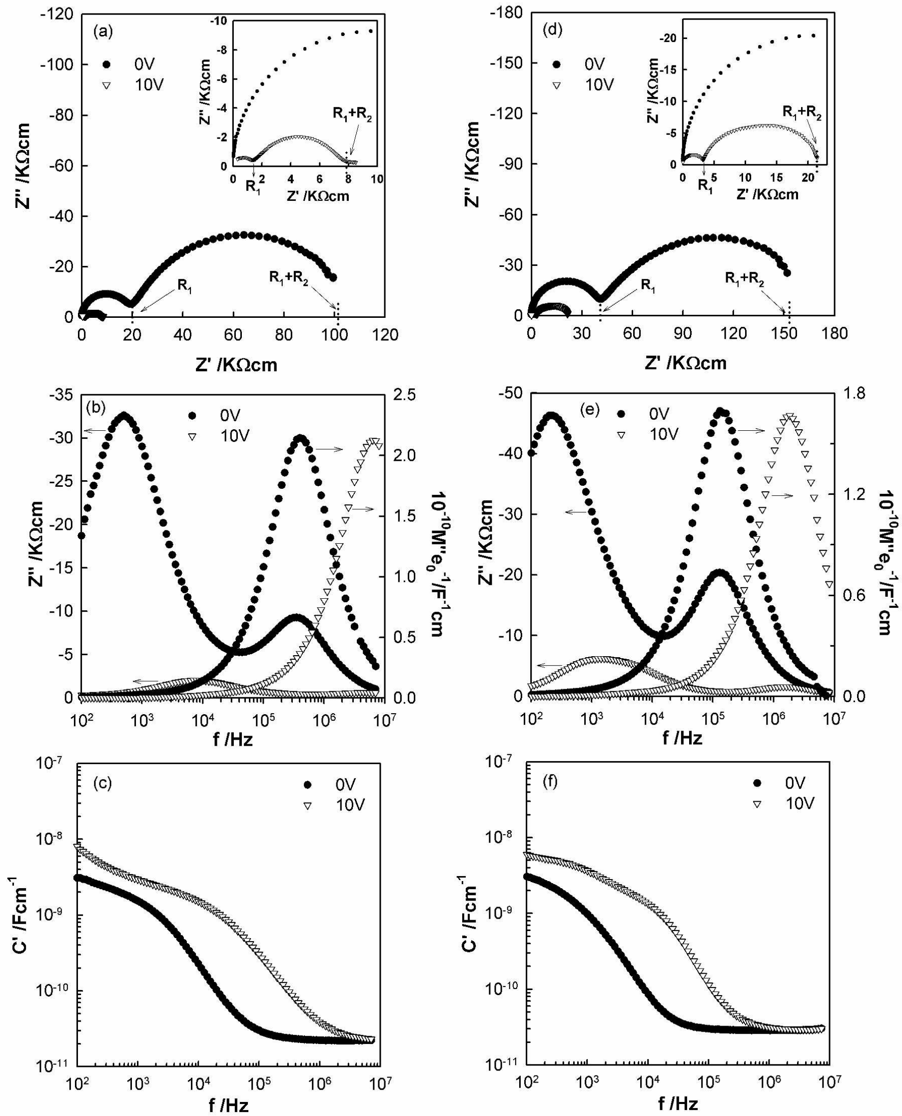

671x791mm (150 x 150 DPI)

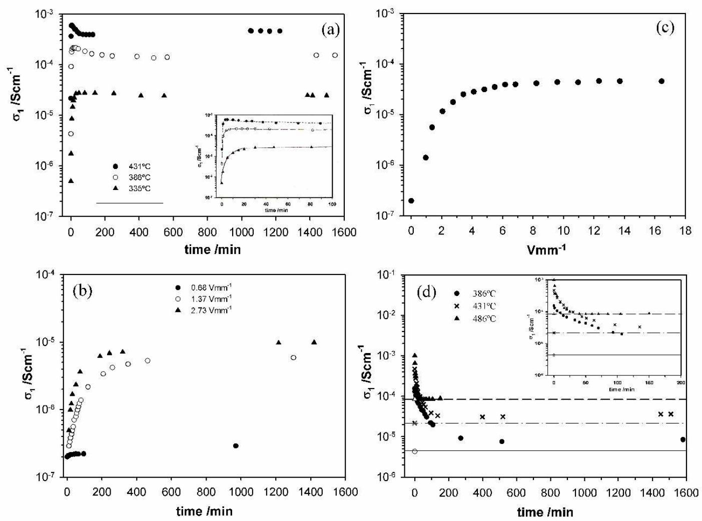

671x1134mm (150 x 150 DPI)

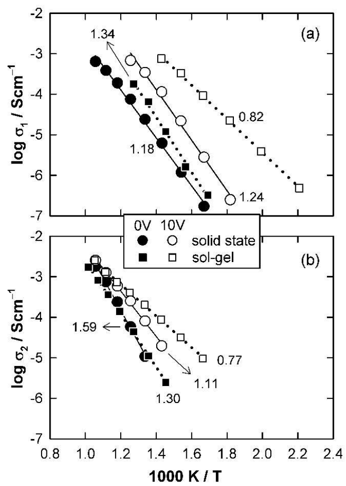

339x1187mm (150 x 150 DPI)

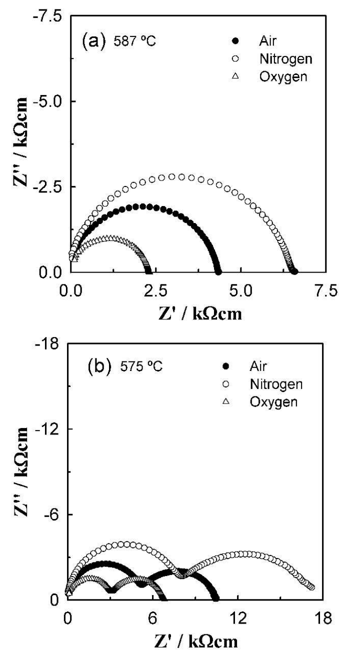

335x1187mm (150 x 150 DPI)

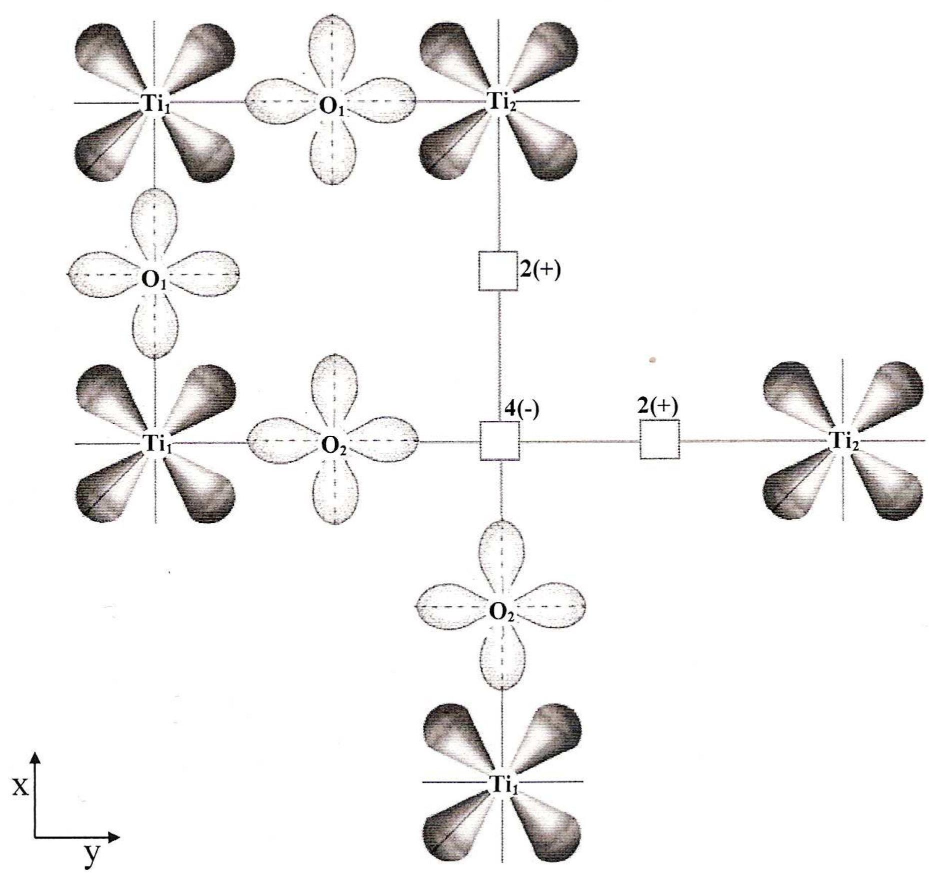

117x110mm (300 x 300 DPI)